EUROPEAN ORGANIZATION FOR NUCLEAR RESEARCH
CERN - ACCELERATORS AND TECHNOLOGY SECTOR

CERN-ATS-2013-047

Heat Transfer through Cable Insulation of Nb–Ti Superconducting Magnets Operating in He II

P.P. Granieri[a,b],
a TE Department, CERN, Geneva, Switzerland
b Swiss Federal Institute of Technology (EPFL), Particle Accelerator Physics Laboratory (LPAP), Lausanne, Switzerland

The operation of Nb–Ti superconducting magnets in He II relies on superfluidity to overcome the severe thermal barrier represented by the cable electrical insulation. In wrapped cable insulations, like those used for the main magnets of the Large Hadron Collider (LHC) particle accelerator, the micro-channels network created by the insulation wrappings allows to efficiently transfer the heat deposited or generated in the cable to the He bath.

In this paper, available experimental data of heat transfer through polyimide electrical insulation schemes are analyzed. A steady-state thermal model is developed to describe the insulation of the LHC main dipole magnets and the Enhanced Insulation proposed for the High Luminosity LHC upgrade (HL-LHC), according to the relevant geometric parameters. The model is based on the coupled mechanisms of heat transfer through the bulk of the dielectric insulation and through micro-channels between the insulation tapes.

A good agreement is found between calculations and tests performed at different applied pressures and heating configurations. The model allows identifying the heat fluxes in the cable cross-section as well as the dimensions of the micro-channels. These dimensions are confirmed by microscope images of the two insulations schemes.

Published in "Cryogenics", 53 (2013) 61-71

Geneva, Switzerland

July 2013

Cryogenics 53 (2013) 61–71

Contents lists available at SciVerse ScienceDirect

Cryogenics

journal homepage: www.elsevier.com/locate/cryogenics

Heat transfer through cable insulation of Nb–Ti superconducting magnets operating in He II

P.P. Granieri *

TE Department, CERN, Geneva, Switzerland
Swiss Federal Institute of Technology (EPFL), Particle Accelerator Physics Laboratory (LPAP), Lausanne, Switzerland

ARTICLE INFO

Article history:
Available online 27 June 2012

Keywords:
Accelerator superconducting magnets
Cable electrical insulation
Heat transfer
LHC
Micro-channels
Superfluid helium

ABSTRACT

The operation of Nb–Ti superconducting magnets in He II relies on superfluidity to overcome the severe thermal barrier represented by the cable electrical insulation. In wrapped cable insulations, like those used for the main magnets of the Large Hadron Collider (LHC) particle accelerator, the micro-channels network created by the insulation wrappings allows to efficiently transfer the heat deposited or generated in the cable to the He bath.

In this paper, available experimental data of heat transfer through polyimide electrical insulation schemes are analyzed. A steady-state thermal model is developed to describe the insulation of the LHC main dipole magnets and the Enhanced Insulation proposed for the High Luminosity LHC upgrade (HL-LHC), according to the relevant geometric parameters. The model is based on the coupled mechanisms of heat transfer through the bulk of the dielectric insulation and through micro-channels between the insulation tapes.

A good agreement is found between calculations and tests performed at different applied pressures and heating configurations. The model allows identifying the heat fluxes in the cable cross-section as well as the dimensions of the micro-channels. These dimensions are confirmed by microscope images of the two insulations schemes.

1. Introduction

Superconducting accelerator magnets are confronted with heat deposit and heat generation due to several mechanisms such as beam losses and AC losses, respectively. An efficient heat extraction from the coil is required to maintain the superconducting state, in particular to overcome the highest thermal resistance between cables and cooling bath that is represented by the cable electrical insulation [1,2].

In the Nb–Ti conductors constituting the main magnets of the Large Hadron Collider (LHC), the choice of superfluid helium (He II) coolant and of a porous insulation scheme allowed improving the heat transfer [3] with respect to sealed insulation schemes as that of the Superconducting Super Collider [4]. In case of the foreseen High Luminosity LHC (HL-LHC) upgrade, the required magnets will have to withstand larger heat loads than in the current LHC operation [5]. For this reason they will make use either of the Nb_3Sn technology that provides a large temperature margin, or of the Nb–Ti technology featuring an increased heat extraction capability thanks to a thermally enhanced insulation scheme [6,7].

So far the thermal characterization of electrical insulations of superconducting cables has been mainly addressed using the *stack method*, an experimental setup reproducing the coil configuration. This kind of measurement was first performed at CEA-Saclay using solid conductors during the R&D phase of the LHC main magnets [3,8], as well as at KEK using resistive cables with the same geometry of the superconducting ones to study the LHC MQXA interaction region quadrupole [9,10]. These tests highlighted the presence of a direct He II link between cables and bath. Heat transfer tests carried out at CERN [11] concerned in a first stage the analysis of high ramp rate quench data of 1 m long LHC model dipoles. In a second stage, tests were carried out on a smaller scale setup, closer to the CEA and KEK mentioned ones. The sample was in this case a segment from a (superconducting) LHC production coil. More recently, stacks made of resistive cables were used at CERN to assess the enhanced thermal behavior of the HL-LHC insulation with respect to the LHC one, with particular attention to the effect of the applied pressure [12,13]. The results of such recent measurements are analyzed in the paper. The different experimental setup used in [14], rather than considering the entire heat transfer in a stack, focused on a simplified one-dimensional heat transfer. This allowed a first decoupled modeling of the polyimide and helium heat transfer contributions.

* Tel.: +41 227676277.
E-mail address: pier.paolo.granieri@cern.ch

0011-2275/$ - see front matter © 2012 Elsevier Ltd. All rights reserved.
http://dx.doi.org/10.1016/j.cryogenics.2012.06.007

The work presented in this paper aims at extending the latter quantitative method. We aim at understanding the mechanisms of heat transport occurring in Nb–Ti cable insulations in order to describe the coil thermal behavior. A simple thermal model accounting for anisotropic three-dimensional coupled heat transfer mechanisms was developed. It is focused on the superfluid helium region, where the strands temperature is below the λ temperature T_λ. The model allows to reproduce He II stack measurements and to determine the heat fluxes distribution. The insulation characteristic dimensions are also identified, and confirmed by microscope images of the insulation tapes deformed under pressure. This modeling approach is applied to the two polyimide insulation schemes of interest for the current and future exploitation of the LHC particle accelerator, hereafter referred to as LHC and HL-LHC insulation schemes.

2. Experimental setup

In this section we briefly introduce the experimental setup and test procedure of the measurements analyzed in the paper. A detailed description can be found in [12,13]. Cu–Ni (Cu-10 wt% Ni) resistive cables were used instead of the Nb–Ti superconducting ones. They feature the same Rutherford geometry as the inner layer cables of the LHC main dipoles [15]. They are made of 28 strands with a diameter of 1.065 mm. They have a width of 15.1 mm and a mid-thickness of 1.9 mm. The cables were insulated according to the schemes described in Sections 4 and 5. A rectangular stack of six cables was made for each insulation scheme, by alternately piling up the cables to compensate for the keystone angle. The stacks underwent a curing cycle at a pressure of 130 MPa and a temperature of 190 °C. An example of cured stack is shown in Fig. 1(top). The sample was instrumented with an array of Au-Fe (Au-0.07 at% Fe) vs. Chromel thermo-couple junctions, located in different positions. Fig. 1(bottom) shows an instrumented sample, where the thermo-couples wires can be observed in the central part and the wires for current injection in the cables at the extremities. Fiberglass plates were added on each side of the stack and epoxy plugs at its extremities to prevent transversal and longitudinal parasitic cooling, respectively. The error in the temperature measurement was estimated to be less than 3 mK or 3% of the measured value, whichever is bigger. The error in the power measurement was evaluated to be smaller than 0.1% of the measured value.

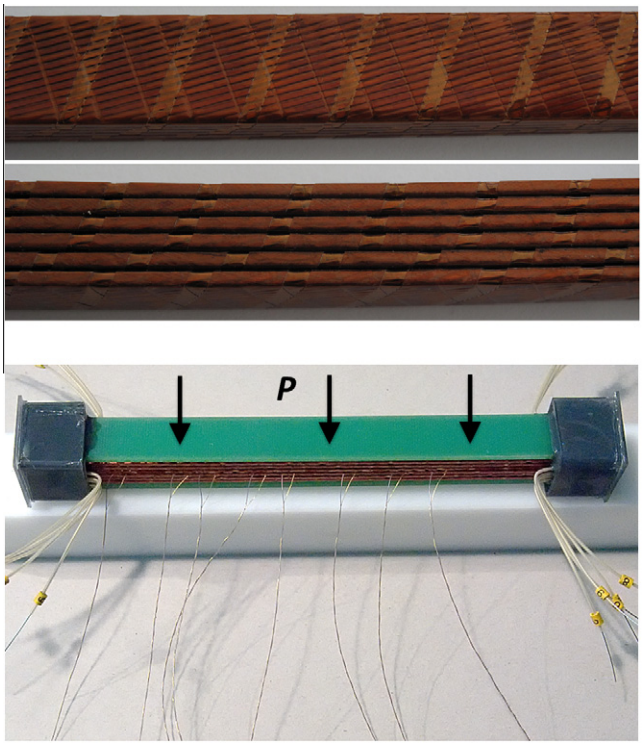

Fig. 1. Top: top and side view of a cured LHC six-units stack. Bottom: instrumented sample. The direction of the applied pressure (P) is also shown.

A compressive pressure was applied on the cables large faces, as schematically shown in Fig. 1(bottom). Both cables small faces are open to the He II bath, which is pressurized at 0.1 MPa and kept at 1.9 K, stabilized within 0.2 mK. Because of the differential thermal contractions between the materials constituting the stack and the sample holder, the pressure applied at room temperature results in a slightly higher pressure at low temperature. In the following we will refer to the pressure applied at room temperature. Either one, three or five cables were uniformly heated by Joule effect, while their steady-state temperature difference with respect to the bath was measured.

3. Model description

The experimental setup is simulated by a network model where steady-state heat transfer balance equations are solved at the nodes. The model is two-dimensional and describes the cables cross-section. Indeed the Joule heating dissipated in the cable is uniform in the longitudinal direction and the epoxy plugs at the sample extremities prevent from parasitic cooling in that direction, so that heat is transversally extracted from the cable. Furthermore it was observed [13] that all the thermo-couple junctions located in different cable cross-sections measure the same temperature below T_λ, due to the superfluid helium filling the interstices among the strands. Therefore the strands temperature is the same for every sample cross-section, which justifies the two-dimensional hypothesis.

However the temperature gradients between the outer strands surface and the external bath develop in the three spatial directions. The model is developed to take into account the three-dimensional shape of the helium channels and their thermal coupling to the insulation tapes, through the definition of nodes in the cable insulation.

The mentioned experimental evidence of equal temperature measured in the different thermo-couple locations below T_λ also means a uniform strands temperature over the cable cross-section. This allows describing all the strands by a single node. The heat transfer between adjacent nodes can occur through polyimide solid conduction, superfluid (He II) conduction or both contributions in parallel. The simplified implementation of the coupling between these thermal mechanisms, as well as the location of the nodes in the insulation, depend on the insulation scheme and will be specifically addressed in Sections 4.1 and 5.1. In this section we define how every contribution is calculated and we discuss the model hypotheses and limits.

The polyimide conduction heat transfer $Q_{pol.}$ is calculated with the Fourier law. The linearity of the polyimide thermal conductivity in the considered temperature range allows to approximate its integral with an average value:

$$Q_{pol} = \sum_{i=1}^{P} \frac{A_{pol.i}}{\delta_{pol.i}} \int_{T_j}^{T_k} k_{pol.}(T)dT \approx \sum_{i=1}^{P} \frac{A_{pol.i}}{\delta_{pol.i}} \bar{k}_{pol.av}(T_j, T_k) \cdot (T_k - T_j). \quad (1)$$

T_j and T_k are the temperatures of two adjacent nodes, $k_{pol.}$ is the temperature dependent polyimide thermal conductivity and $\bar{k}_{pol.av}(T_j, T_k)$ is the average value between T_j and T_k. P is the number

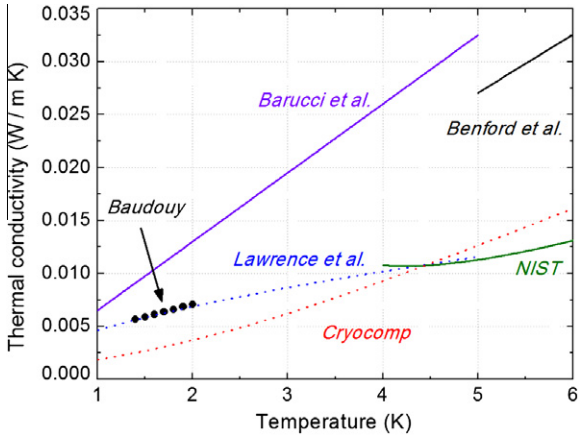

Fig. 2. Polyimide thermal conductivity at low temperature, compiled from different sources [16–21].

of insulation portions between nodes j and k having surface $A_{pol.i}$ and thickness $\delta_{pol.i}$.

The polyimide thermal conductivity at low temperature was investigated by several authors, as summarized in Fig. 2. Data from Baudouy [16] in the superfluid region agree with those from Lawrence et al. [17] that are taken over a larger temperature range. Furthermore data from Lawrence et al. and from NIST [18], which refer to two different temperature ranges, are in agreement in the overlap of the two ranges. In the following we will retain values from Baudouy rather than from Cryocomp [19] or Barucci et al. [20]. The latter differ by a factor two below T_λ and to our knowledge there are not other experimental values confirming them. The sensitivity of the model to the polyimide thermal conductivity was assessed. Assuming different values than those from [16], the results of the computations do not change by more than 10%.

As for the heat transport through the micro-channels located between the insulation tapes, we assume that it follows the known laws of the superfluid dynamic regimes. However a complete study assessing whether these macro-scale laws are valid in such narrow channels is missing. The validity of the classical laminar and turbulent regimes in pressurized He II has been so far only confirmed down to 17 μm thick channels [13,22,23]. Fundamental investigations are ongoing to study possible dependencies on the geometrical size and shape for smaller dimensions [13]. This is mainly of concern for the LHC insulation, since as it will be shown the average size of the channels in the HL-LHC insulation is typically larger.

The integral expressions of the laminar (Landau) and turbulent (Gorter–Mellink) equations are implemented in the numerical model. In particular the Landau heat flux Q_{Lan} is calculated as:

$$Q_{Lan} = \sum_{i=1}^{N} \frac{A_{ch.i} \cdot d_{ch.i}^2}{l_{ch.i}} \int_{T_j}^{T_k} \frac{[\rho(T) \cdot s(T)]^2 \cdot T}{\beta \cdot \eta(T)} dT, \tag{2}$$

where ρ is the density of the bulk helium, s the entropy, T the temperature, η the viscosity and β is a coefficient depending on the channel cross-section. N is the number of channels between nodes j and k featuring surface $A_{ch.i}$, length $l_{ch.i}$ and diameter $d_{ch.i}$ (if circular). In the considered case of channels rectangular cross-section with sides $a_{ch.i}$ and $b_{ch.i}$, the relation between normal fluid velocity, pressure and temperature gradient [24,25] yields a β of 12 and a $d_{ch.i}$ expressed as a combination of $a_{ch.i}$ and $b_{ch.i}$:

$$d_{ch.i} = \sqrt{\frac{a_{ch.i} \cdot b_{ch.i}}{b_{ch.i}/a_{ch.i} + a_{ch.i}/b_{ch.i}}}. \tag{3}$$

The Gorter–Mellink heat flux Q_{GM} is calculated as:

$$Q_{GM} = \sum_{i=1}^{N} \frac{A_{ch.i}}{l_{ch.i}^{1/3}} \left[\int_{T_j}^{T_k} \frac{\rho_s(T)^3 \cdot s(T)^4 \cdot T^3}{A_{GM}(T) \cdot \rho_n(T)} dT \right]^{1/3} = \sum_{i=1}^{N} \frac{A_{ch.i}}{l_{ch.i}^{1/3}} \left[\int_{T_j}^{T_k} f(T) dT \right]^{1/3}, \tag{4}$$

where ρ_n and ρ_s are the density of the superfluid and of the normal components respectively, A_{GM} is the Gorter–Mellink coefficient and f is the He II equivalent thermal conductivity.

The variables ρ, s, η, ρ_s, ρ_n, f and A_{GM} are temperature dependent. Their values come from the HEPAK database [26] with an error typically smaller than 1%. They all refer to a helium pressure of 0.1 MPa.

The transition between the two dynamic regimes of superfluid helium is related to the onset of vorticity in the superfluid and in the normal components. It occurs at a critical heat flux density that depends on the channel dimension. Also in this case, a fundamental study in pressurized He II would be needed, to experimentally determine the critical heat flux density in such small dimensions [13]. In the following we will use the critical heat flux density Q_{c1} predicted by Ladner and Tough [27]. This critical heat flux is associated to the critical velocity of the superfluid component and is expressed as:

$$Q_{c1} = \frac{4 \cdot \alpha}{\gamma_0(T_{bath}) \cdot D} \cdot \rho_s(T_{bath}) \cdot s(T_{bath}) \cdot T_{bath}. \tag{5}$$

α is an experimentally determined constant value depending on dimension and shape of the tested channels, that is approximately equal to 1. D is the hydraulic diameter and γ_0 is a temperature and geometry dependent parameter, equal to 102 s/cm^2 for a bath temperature T_{bath} of 1.9 K. The other functions ρ_s and s are also evaluated at the same T_{bath}. It is worth noticing that Eq. (5) was determined in saturated He II for particular channel geometries, by making use of empirical coefficients.

The temperature sensors aiming at measuring the strands temperature are electrically insulated from the strands themselves. This results in a measured temperature that lies in between the temperature of the strands and that of the helium inside the cable. Because of the associated uncertainty, we neglected the Kapitza resistance between strands and helium. The polyimide–helium Kapitza resistance is neglected as well, because more than one order of magnitude smaller than the thermal resistance of the polyimide bulk material [16]. The strands-polyimide contact resistance is not considered because of the large associated uncertainty [28].

Although the geometry of the insulation scheme is considered in the model, it is important to stress that a fundamental uncertainty remains on some parameters, mainly the channels cross-section and the presence of possible restrictions along the channels length. Besides the effect of the pressure applied during the test, several other mechanisms can influence the micro-channels topology and dimensions. For instance the curing cycle [29], the plastic deformation due to the applied pressure [30] as well as to creep effect [29], or the stress induced by the differential thermal contractions of the coil components. All these mechanisms affect the micro-channels among the insulation tapes, thus making hard to precisely determine their shape and dimension from a mechanical standpoint. In the following, we will determine the channels average dimensions from a thermal point of view, assuming that they do not vary along the channels length. Because of the mentioned uncertainties, we prefer not to over complicate the modeling.

The steady-state hypothesis allows to assume in each node that the algebraic sum of the heat fluxes exchanged with the other nodes and of the heat sources is zero. All the heat balance equations are written in the form of a matrix system: $H \cdot T = Q$. Each term of the matrix H is the sum of the heat transfer coefficients

associated to the heat fluxes entering or exiting a node. Each row contains all the contributions relative to a single node. T is the vector of the temperatures at the nodes. Q is the vector of the heat sources, where the only terms different from zero are those corresponding to the nodes representing the cables, whether heated.

All the heat flux contributions except the heat sources are temperature dependent, as from Eqs. 1, 2, and 4. Therefore the matrix system is solved by subsequent iterations, as long as the elements of the vector T feature a percentage relative variation smaller than 0.01%. Another iteration loop is present, external to the previous one. It is performed to determine the free parameters of the model that allow reproducing experimental measurements carried out with different heating configurations and different applied pressures. These parameters are the unknown channels dimensions and will be detailed in Section 4.1 for the LHC insulation and in Section 5.1 for the HL-LHC insulation.

4. LHC Insulation

The LHC insulation scheme used for the main dipole magnets is shown in Fig. 3, where some helium heat transfer paths are also highlighted. They will be discussed in the next section.

The geometric parameters of the three wrapped polyimide tapes constituting the insulation are listed in Table 1. The first two tapes ensure the electrical insulation by minimizing the risk of punch-through and providing a sufficiently long surface path for electrical discharge. The 3rd tape is wrapped with a spacing of 2 mm in order to create channels for the He II coolant between the coil turns. Furthermore, the last tape provides cohesion between adjacent cables thanks to a thin layer of polyimide glue on its outer surface that is activated during the curing cycle. It is worth noticing the importance of the development work done to avoid flowing of the polyimide glue [31]. This is a necessary condition for the He II permeability of the analyzed insulations.

4.1. Model implementation

The first two tapes create large aspect ratio micro-channels featuring different thickness whether located on the compressed or on the non-compressed cable face, as shown in Fig. 4. Therefore we distinguish the behavior of the cable large face from that of the cable small face. In the following we will refer to these micro-channels as slits in the cable longitudinal direction having the width of the relevant cable face.

Fig. 5 shows a detailed sketch of the insulation and of the heat transfer paths implemented in the model. The top and bottom pictures refer to the cable small and large face, respectively.

The slits on the cable small face provide the same heat extraction for every pressure applied on the stack, because they are not affected by the pressure applied by the sample-holder. Furthermore they are open to the bath. Their length depends on the tapes overlap, varying between a minimum of 6 mm if they exit on the spacing of the third layer, thus in the external bath (path 1), and a maximum of 11 mm if they exit in the middle of the third layer

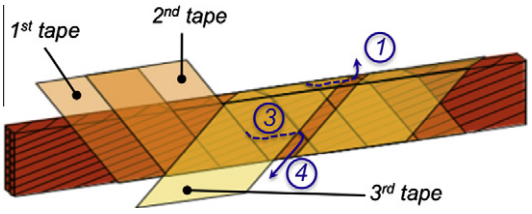

Fig. 3. LHC insulation scheme. Two helium heat transfer path are also shown (see text for description).

Table 1
Geometric parameters of the LHC insulation scheme.

Insulation scheme	1st tape	2nd tape	3rd tape
LHC	11 mm wide No spacing 50 μm thick	11 mm wide No spacing 50 μm thick 50% overlap 1st tape	9 mm wide 2 mm spacing 69 μm thick Cross wrapped

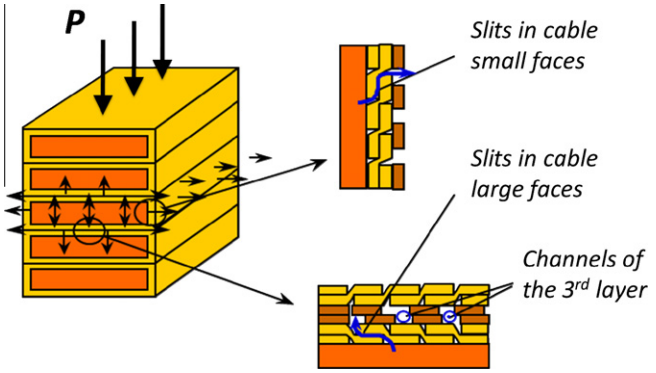

Fig. 4. Sketch of the LHC insulation slits on the cable small and large faces, in the stack setup (from [32]).

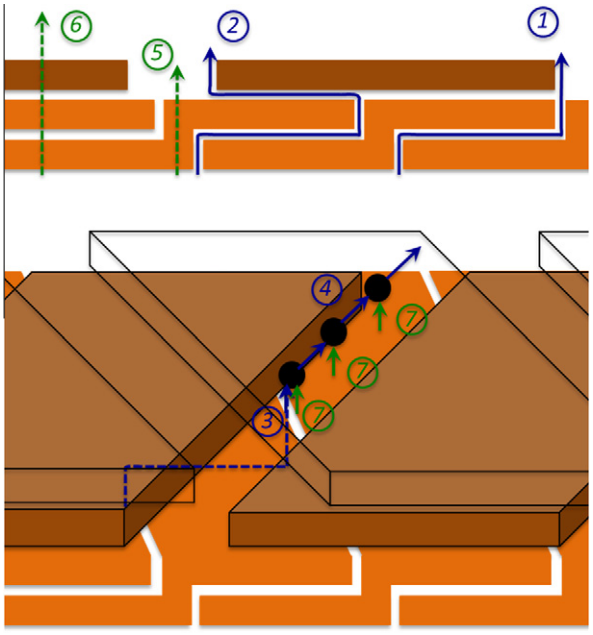

Fig. 5. Sketch of the heat transfer paths implemented in the LHC model, where the black balls represent the nodes. The top picture refers to the cable small face, whereas the bottom picture refers to the cable large face.

(path 2). We calculate the total number of slits from the sample length and the width of the first two tapes. 18% of them are 6 mm long slits. For the remaining longer slits an average length is assumed.

The heat extraction through the cable small face is completed by solid conduction through polyimide, which does not feature any dependence on the applied pressure either. It is the sum of two contributions: conduction through the only first two tapes where the spacing of the third layer is (path 5), and through all the three tapes elsewhere (path 6). According to [32], we assume the polyimide conduction surface equal to the total surface with

two polyimide tapes for the heat path 5, and with three tapes for the heat path 6. The considered thickness is 100 μm for heat path 5 and 169 μm for heat path 6.

The cable small face is the only one for which it is assumed that He II and polyimide conduction heat transfer are decoupled. This hypothesis was demonstrated to be consistent in [14].

The description of the cable large face is more elaborate. The length of the slits is the same as before, whereas their thickness depends on the applied pressure. The slits (heat path 3) are not directly open to the bath, but to the channels located in the 2 mm spacing of the third layer. These third layer channels are in contact with the bath at their extremities, through the heat paths 4. Polyimide heat transfer between the cables and the third layer channels along their length is also taken into account, through the first two insulation tapes (heat path 7). The above mentioned hypotheses on the polyimide conduction surface and thickness are made here as well. As depicted in Fig. 5 (below), several nodes are defined to describe the link between slits and third layer channels, as well as the coupling between He II and polyimide heat transfer. The model accounts for the possibility that the He II link between slits and third layer channels might occur in each of the three nodes shown (for each half cable width), calculating the corresponding surface.

The polyimide heat path 8 allows a direct coupling of adjacent cables through the contact surface between their third tapes, as well as a link between one cable and the third layer channels of its adjacent cable, through their relevant surfaces. The compressed insulation thickness on the large cable face is derived from the mechanical measurements reported in [29].

Several other nodes are defined: they correspond to the cables where the heat can be deposited, and to the bath that is kept at a constant temperature of 1.9 K.

Fig. 6 shows the simplified sketch of the model cross-section, where all the six cables of the measured stack are described. It is worth underlining that, although the sketch refers to the cables cross-section, the third spatial direction is taken into account:

- to describe the slits in the cable longitudinal direction and the third layer channels, as explained;
- to consider all the slits, channels and polyimide surfaces along the sample length, which are lumped in one single cross-section.

The unknown dimensions, which constitute free parameters of the model, are:

a. the thickness of the slits in the cable small faces: th_{small};
b. the cross-section of each slit in the cable large faces: A_{large};
c. the cross-section of the third layer channels. This parameter $A_{channel}$ will be expressed in terms of percentage of the non-pressed channels cross-section, i.e. 2 mm × 69 μm.

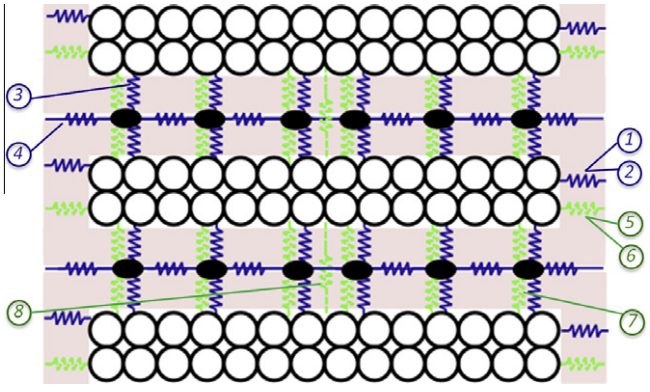

Fig. 6. Sketch of the model developed for the LHC insulation. The black ovals are the nodes. The dark blue resistances represent the helium heat paths, whereas the light green resistances represent the polyimide heat paths.

4.2. Results

The results are presented in terms of temperature increase as a function of the power dissipated in the 156 mm long central conductor, in a pressurized He bath at 1.9 K. The first results shown in Fig. 7 are obtained with a simplified model not considering the slits in the cable large faces. Calculations are compared to measurements in case of two heating configurations: one heated cable (the central one) and five heated cables. The choice of the same optimized values for th_{small} and $A_{channel}$ does not allow reproducing both measurements: if the calculation is in good agreement with the measurement for the five heated cables case, some heat removal is missing in the one heated cable case. Adding the slits in the cable large faces provides a solution to this problem, since the corresponding heat extraction is larger if the cables adjacent to the central one are not heated. It is worth noticing that heat transfer measurements from a stack sample already provided qualitative information on the mechanisms occurring in the cable large faces [13]. They proved that the helium penetrating the void spaces between adjacent cables plays a role in the cable cooling.

Fig. 8 reports results obtained with the full model described in the previous subsection, compared to measurements performed at an applied pressure of 50 MPa. Good agreement is found for the different heating configurations, with the following choice of the unknown parameters:

- th_{small} = 6.64 μm;
- A_{large} = 1.69 μm^2;
- $A_{channel}$ > 10%.

The small value of A_{large} is associated to a regime of pure superfluidity, as it will be shown, that allows an extremely larger heat transfer than in other regimes. It is useful to remind that such value is obtained in the assumption of a constant cross-section along the channel length. In case of the large (pressed) cable face this hypothesis is not as reliable as for the small (non-pressed) face, because the channels will feature several and important restrictions. A_{large} has to be considered as the equivalent cross-section under the mentioned assumptions. It is worth noticing that larger values of $A_{channel}$ do not substantially modify the results of the calculation,

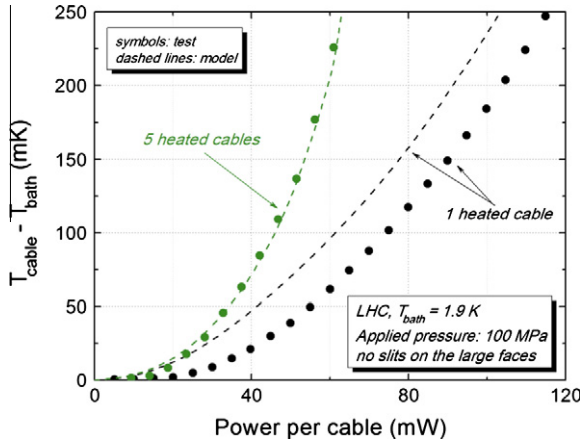

Fig. 7. Heat transfer curves through the LHC insulation for different heating configurations, simplified model without channels in the cable large faces (curves) vs. measurements (markers).

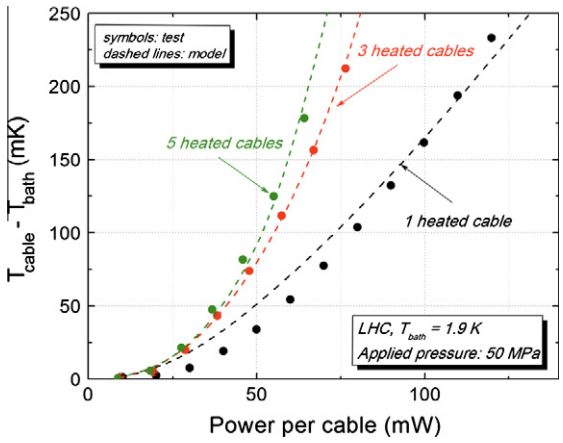

Fig. 8. Heat transfer curves through the LHC insulation for different heating configurations, model (curves) vs. measurements (markers).

since the bottleneck of the heat extraction through the cable large faces is represented by the He II and polyimide heat transport towards the channels of the third layer.

The different heat fluxes exiting the cable can be grouped into the following contributions:

- He II through cable small faces (heat paths 1 and 2);
- Polyimide conduction through the cable small faces (heat paths 5 and 6);
- He II through the cable large faces towards the third layer channels (heat path 3);
- Polyimide conduction through the cable large faces towards the third layer channels (heat path 7);
- Polyimide conduction between adjacent cables (heat path 8).

Fig. 9 reports such contributions, in case of three heated cables compressed at 50 MPa. The He II heat flux through the cable small faces is the largest contribution. It represents more than 60% of the total heat extraction for small temperature increase. It tends towards a vertical asymptote while approaching T_λ, and its relative contribution decreases to 50%. The polyimide conduction through the cable small faces and between adjacent cables is small, whereas the two mechanisms of heat transfer to the channels of the third layer in the cable large faces play a non-negligible role. In particular, the polyimide contribution through the cable large faces represents 20% of the total heat extraction. The critical heat flux delimiting the Landau from the Gorter–Mellink region is estimated to be 16 mW for the slits of the cable small faces and 100 mW for those of the cable large faces. This means that the He II heat transfer is always described by Eq. (4) for the slits of the cable small faces and by Eq. (2) for the slits of the cable large faces.

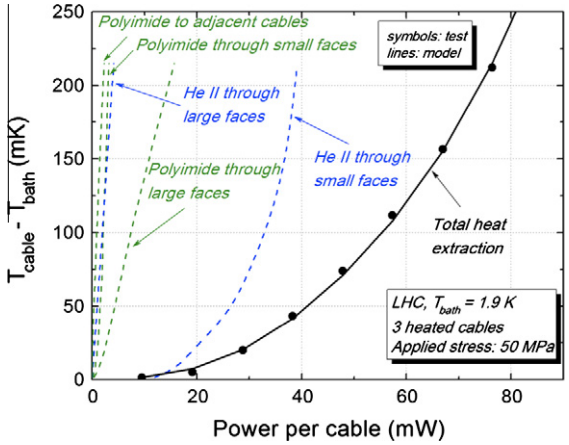

Fig. 9. Contributions to the heat extraction through the LHC insulation.

Fig. 10 presents the case of three heated cables for different applied pressures. The same th_{small} of 6.64 μm is used in all cases, because it does not depend on the pressure. The other parameters decrease while increasing the pressure, as reported in Table 2. In general the agreement between the LHC model and the relevant measurements is within 7%, except for the one heated cable configuration where the error can be larger below a temperature increase of 100 mK.

4.3. Slits on the cable small and large faces

Stacks made of two insulated cables were prepared in order to visualize their electrical insulation under the microscope [13]. The two-units stacks were cured according to the cycle mentioned in Section 2 and inserted inside a small sample holder to apply a pressure of around 50 MPa at room temperature. A cut of sample and sample holder was realized in the cable transversal direction, and the cross-section was then polished.

The pictures reported in Fig. 11 are details of the cable small faces, where the strands and the slits between the tapes can be clearly identified. They feature a not constant thickness ranging approximately from 3 to 18 μm, which is in agreement with the theoretical thickness of around 7 μm determined through the modeling.

Fig. 12 shows two details of the insulation on the pressed cable large faces. It is possible to distinguish some slits between the tapes, as those assumed in the model. However, they are far from featuring a constant shape and thickness. This observation qualitatively confirms hypotheses and results of the model developed for the LHC insulation.

5. HL-LHC insulation

The HL-LHC insulation scheme is shown in Fig. 13. It is made of three wrapped polyimide tapes which geometric parameters are listed in Table 3.

Compared to the three tapes of the LHC insulation scheme, the role of the second tape in this scheme is not to provide electrical insulation, but spacing between the other tapes. This creates a structure more open to He II. The electrical insulation function is taken over by the third tape, which is overlapped with respect to the first one. The last tape features also in this case a thermally

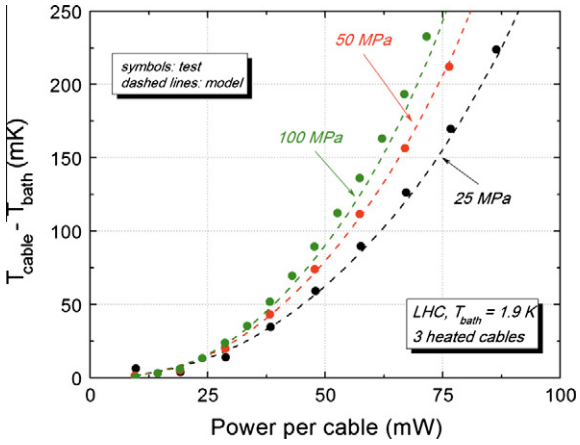

Fig. 10. Heat transfer curves through the LHC insulation for different applied pressures, model (curves) vs. measurements (markers).

Table 2
Summary of the average slits and micro-channels dimensions for the LHC insulation. They were determined with the developed model as a function of the applied pressure.

Insulation scheme	Slits/channels	25 (MPa)	50 (MPa)	100 (MPa)
LHC	th_{small}	6.64 μm	6.64 μm	6.64 μm
	A_{large}	1.72 μm^2	1.69 μm^2	1.63 μm^2
	$A_{channel}$	>20%	>10%	>5%

activated adhesive film on its external part to provide the coil with mechanical stability. Breakdown voltage measurements on cables stacks showed satisfactory electrical performance of this insulation scheme [23].

5.1. Model implementation

The main innovations of the HL-LHC scheme are the channels created along the second tape, as well as the openings between first and second layer and between second and third layer. This provides a large direct path through He II from the strands to the bath.

The mentioned channels, hereafter referred to as second layer channels, are 9.5 mm long. They can either come out in the cable small face (heat path 1), hence directly to the bath, or in the cable large face (heat path 2). In the latter case a supplementary channel length has to be considered before reaching the bath, along the edges of the third tape (heat path 3). We will refer to this supplementary length as to third layer channels. The total length between strands and bath through second and third layer channels can reach a maximum of 17.4 mm. These He II heat paths are presented in Fig. 13.

Every second layer channel lies on the cable large faces for most of its length. In this zone it is submitted to the pressure applied on the stack, hence all the channels feature the same minimum cross-section. For this reason, unlike what we did for the LHC insulation, the heat transfer contribution of the large face will not be differentiated from that of the small face.

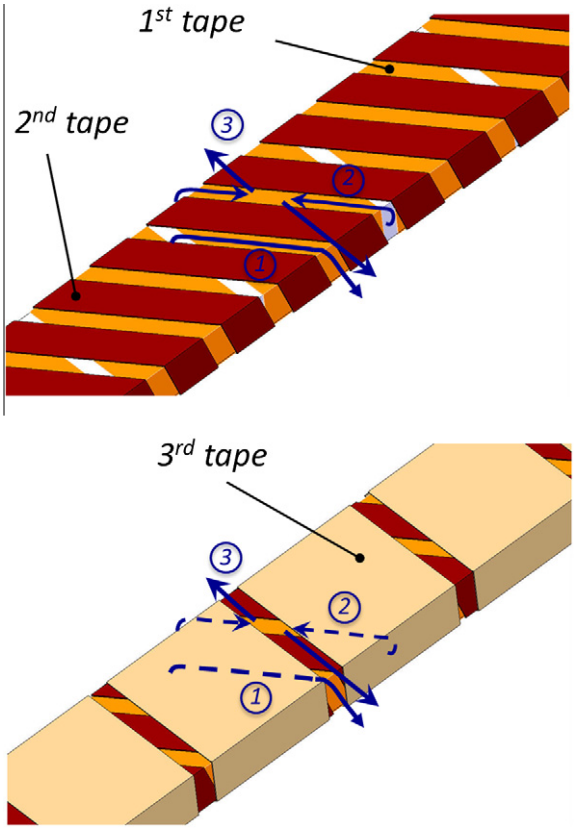

Fig. 13. HL-LHC insulation scheme. The main helium heat transfer path are also shown (see text for description).

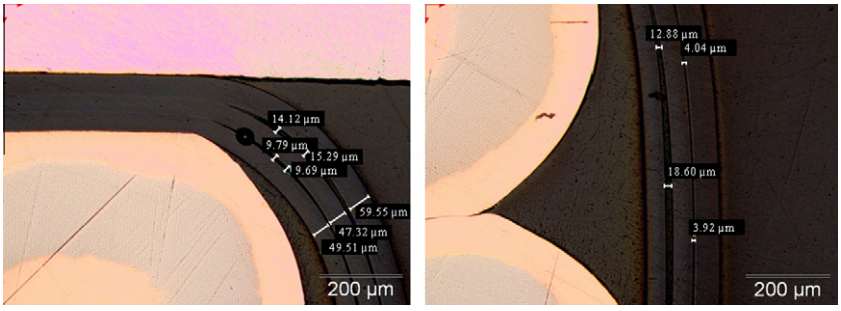

Fig. 11. Slits in the LHC insulation scheme located on the cable small faces. Left: insulation around a strand located between the cable small and large face. Right: insulation close to strands in the cable small face.

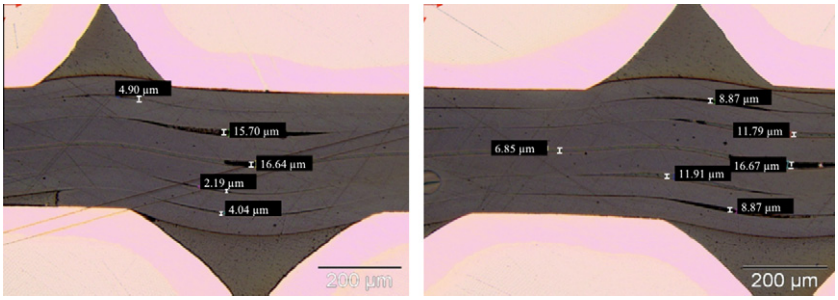

Fig. 12. Slits in the LHC insulation scheme located on the cable large faces.

Table 3
Geometric parameters of the HL-LHC insulation scheme.

Insulation scheme	1st tape	2nd tape	3rd tape
HL-LHC	9 mm wide 1 mm spacing 50 μm thick	3 mm wide 1.5 spacing 75 μm thick Cross wrapped	9 mm wide 1 mm spacing 69 μm thick 50% overlap 1st tape

The choice of not separating the thermal behavior of small and large cable faces has also a physical meaning. The described helium heat transfer paths run indeed around the cable, concerning at the same time its small and large faces. This is confirmed by the results of the heat transfer tests performed in [33], through a setup aimed at reproducing the behavior of the only compressed large face. The measurements performed in such conditions show a small improvement of heat transfer through the HL-LHC insulations with respect to the LHC insulation, of around 25%. This is much smaller than the major improvement measured in [12] through the *stack method*. Small and large cable faces must therefore work together to fully exploit the He II open structure of the HL-LHC insulation.

Fig. 14 shows a detailed sketch of the insulation and of the heat transfer paths implemented in the model. Both the second layer channels (helium heat path 1 or 2) and the third layer channels (helium heat path 3) are described. 12% of the second layer channels exit directly in the bath. The remaining ones are coupled to the third layer channels.

A node is defined in the middle of the second layer channels, to consider the coupling with the polyimide heat transfer occurring through the first insulation tape (heat path 4). Other nodes are defined along the third layer channels. They account for heat deposit along their length due to:

- helium second layer channels (heat paths 1 and 2);
- polyimide conduction through the first insulation tape (heat path 4);
- polyimide conduction through the first and second insulation tapes (heat path 5).

The model accounts for the possibility that the He II link between second and third layer channels might occur in each of the 3 nodes shown in Fig. 14 (for each half cable width), calculating the corresponding surface. The remaining nodes concern the link between polyimide conduction and third layer channels. This feature of the model is schematically shown in Fig. 15, in the heat transfer paths shown above and below the strands.

Two more nodes are defined, corresponding to the cable strands and to the 1.9 K external bath. The polyimide solid conduction contributions through the cable small face, as well as towards the adjacent cables, are implemented. The geometrical insulation thickness (of either two or three tapes) is considered for the small face. The average compressed insulation thickness, derived from the measurements reported in [29], is used for the large face.

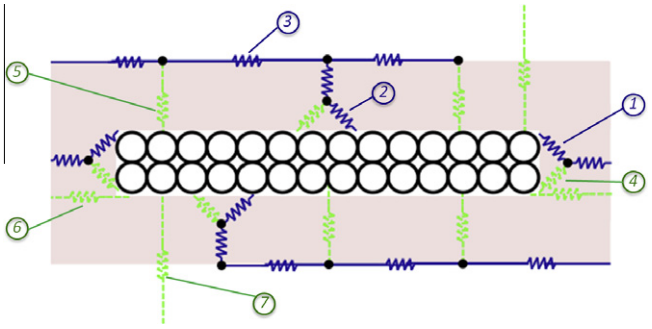

Fig. 15. Sketch of the model developed for the HL-LHC insulation. The black circles are the nodes. The dark blue resistances represent the helium heat paths, whereas the light green resistances represent the polyimide heat paths. (For interpretation of the references to color in this figure legend, the reader is referred to the web version of this article.)

The slits in the cable longitudinal direction, that were considered for the LHC insulation, are neglected in this case because noticeably smaller than the second layer channels.

It was shown in [12] that adjacent cables insulated with the HL-LHC scheme are thermally decoupled to each other well above T_λ. A model focusing on one single cable could therefore be developed, assuming the adjacent cables to be at the bath temperature. Its simplified sketch is reported in Fig. 15. As for the LHC model, besides the cable cross-section we also take into account the third spatial direction to describe all the helium channels along their whole length, as well as the coupling with the polyimide conduction mechanism.

The unknown dimension constituting the only free parameters of the model is the cross-section of the second layer channels. The cross-section of the third layer channels is considered to scale accordingly. This parameter $A_{channel}$ is expressed in terms of percentage of the non-pressed channel cross-section, i.e. 1.5 mm $\times$ 75 μm.

5.2. Results

Fig. 16 reports the results obtained in case of one and five heated cables, compared to measurements performed at an applied pressure of 50 MPa. A good agreement is found with an $A_{channel}$ of 39% in the five heated cables case and of 44% in the one heated cable case. This difference is due to the fact that, in the one heated cable case, the central conductor can profit of the channels network of its cold adjacent cables. Therefore the actual channels cross-section should be estimated in the five heated cables case.

The different heat fluxes exiting the cable can be grouped into the following contributions:

- He II through the second layer channels (heat paths 1 and 2);
- Polyimide conduction through the first tape to the middle of the second layer channels (heat path 4);

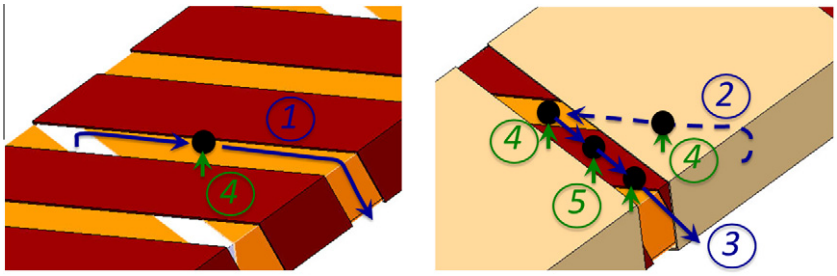

Fig. 14. Sketch of the heat transfer paths implemented in the HL-LHC model. The black balls represent the nodes.

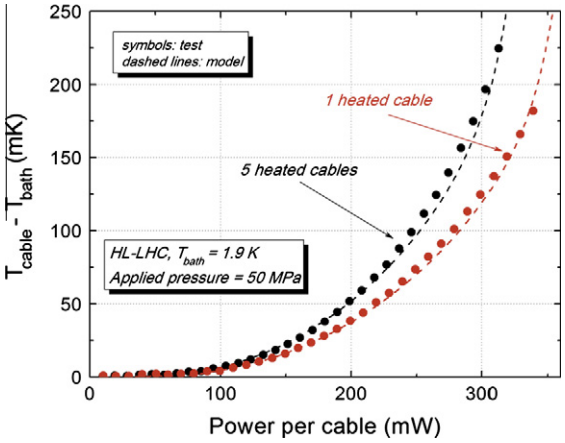

Fig. 16. Heat transfer curves through the HL-LHC insulation for different heating configurations, model (curves) vs. measurements (markers).

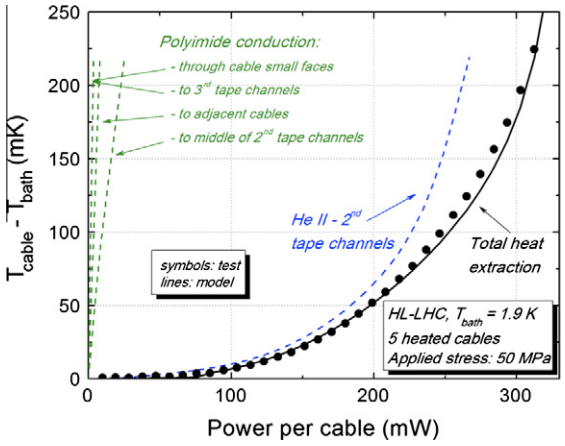

Fig. 17. Contributions to the heat extraction through the HL-LHC insulation.

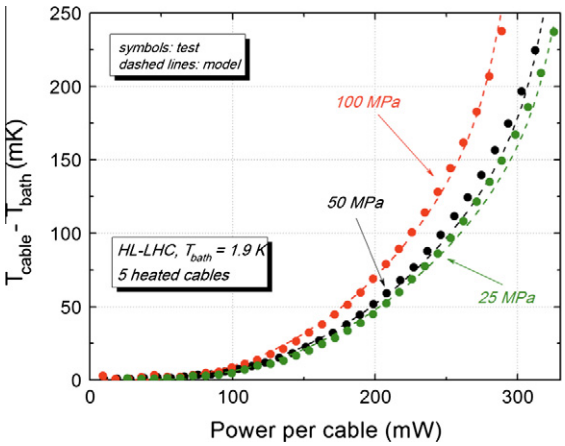

Fig. 18. Heat transfer curves through the HL-LHC insulation for different applied pressures, model (curves) vs. measurements (markers).

- Polyimide conduction through first and second tape to the third layer channels (heat path 5);
- Polyimide conduction through cable small faces (heat path 6);
- Polyimide conduction between adjacent cables (heat path 7).

Table 4
Summary of the average micro-channels dimensions for the HL-LHC insulation. They were determined with the developed model as a function of the applied pressure.

Insulation scheme	Channels	25 MPa	50 MPa	100 MPa
HL-LHC	$A_{channel}$	41%	39%	35%

Fig. 17 reports such contributions, in case of five heated cables compressed at 50 MPa. The He II heat flux through the second layer channels is by far the largest contribution, representing 90% of the total heat extraction. The critical heat flux delimiting the Landau from the Gorter–Mellink regime is estimated to be 36 mW through Eq. (5), thus confirming the establishment of a fully developed turbulent regime. The polyimide heat fluxes have a minor impact. Among them, the most significant one is that through the first tape to the middle of the second layer channels. It represents less than 10% of the total heat extraction.

Fig. 18 presents the case of five heated cables for different applied pressures. The $A_{channel}$ values that better fit the experimental data are reported in Table 4. $A_{channel}$ decreases while increasing the pressure, and is sufficiently large even at the highest pressures required for magnet operation. In general the agreement between the HL-LHC model and the relevant measurements is within 6%.

The average channels cross-section obtained with the presented thermal model is comparable to that obtained with similar models on other variants of HL-LHC insulations [34,35], albeit not validated for the different mechanical and heating configurations tested. A finite elements model was also developed to investigate the channel deformation in the HL-LHC scheme from the mechanical point of view [36]. The main approximation of our thermal model is to consider average dimensions for the channels, uniform along their length. As far as the mechanical model is concerned, it does not take into account plastic deformations due for instance to the curing cycle and to creep mechanisms, as well as the stress induced by the differential thermal contractions of the coil components. Despite that, the values of minimum $A_{channel}$ predicted by the mechanical model at 50 and 100 MPa (48% and 39%, respectively) are not far from those determined in this section.

5.3. Micro-channels

The samples for visualizing the HL-LHC insulation were prepared similarly to those described in Section 4.3. The cut direction was in this case perpendicular to the second layer channels of one of the cables.

The pictures in Fig. 19 show details of the insulation in the compressed cable large face (between adjacent cables). It is observed that the second and third layers channels are open in the majority of the cases, though they feature drastic cross-section reduction in few other cases (bottom right picture). In general, the microscopic visualization of the HL-LHC insulation confirms the presence of an extremely open structure, even at high applied pressures. This observation agrees with the large measured and modeled heat extraction. The insulation structure is far from regular, therefore it is worth stressing once more that the channels dimension determined through the thermal model has to be considered as an average cross-section.

We also took images of the cable small faces, where we could observe similar slits as in the LHC insulation scheme (Fig. 11). These slits featured a not constant thickness between approximately 0 and 25 μm. Such dimensions cannot provide an explanation for the large heat transfer capacity of the HL-LHC insulation, as the thermal model also confirmed.

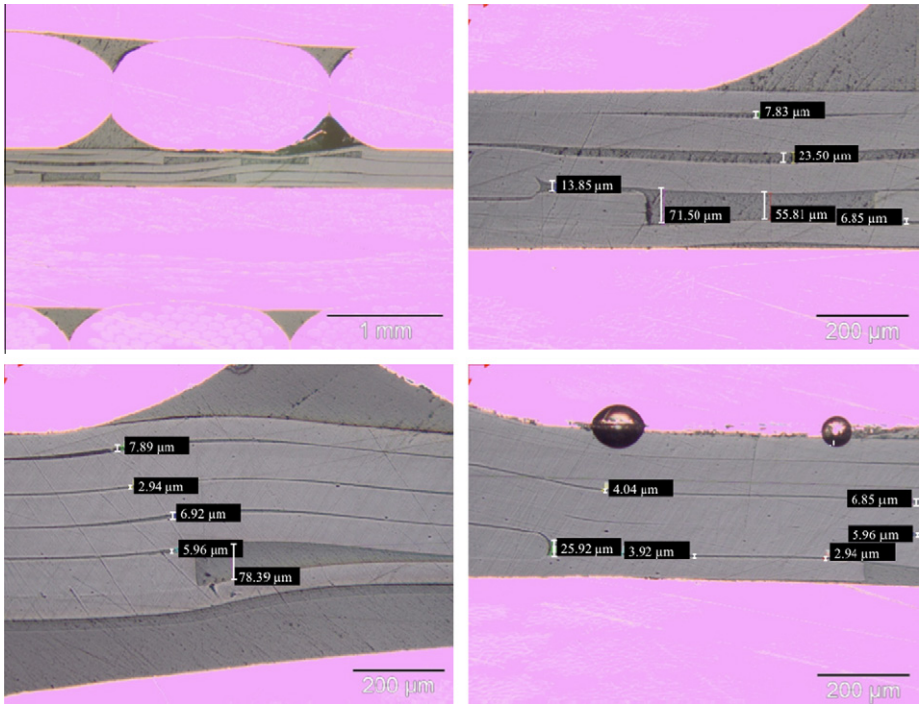

Fig. 19. Micro-channels in the HL-LHC insulation scheme on the cable large faces (between adjacent cables). The top left picture is obtained with a small zoom, whereas a larger enlargement is used for the others.

6. Conclusions

We investigated the thermal behavior of electrical insulations of Nb–Ti superconducting cables cooled by superfluid helium. We developed a theoretical model that allows to quantitatively explain the results of experimental heat transfer tests. By comparison to available experimental measurements performed in different heating configurations and at different applied pressures, the model allowed identifying the main mechanisms for heat extraction in the LHC and HL-LHC insulation schemes. The He II micro-channels were recognized to be the responsible for the most significant heat transfer. Their unknown dimensions were identified from the thermal analysis, and confirmed by microscope images.

In the LHC insulation, the micro-channels consist of slits created by the tapes overlap. They feature an average thickness of about 7 µm in the non-pressed (small) cable faces, permitting the establishment of a turbulent regime. In the pressed (large) cable faces the equivalent cross-section of each slit is smaller than 2 μm^2, resulting in a laminar regime. In the HL-LHC insulation, the micro-channels are located between the wrappings of the intermediate tape. In the mechanical conditions typical of magnet operation they feature an average cross-section of about 40% of their non-pressed geometrical size, which allows the establishment of a fully developed Gorter–Mellink regime.

Acknowledgments

The author wishes to thank all the colleagues who gave a contribution to this work: D. Tommasini for his continuous support and careful advice, D. Richter for sharing with me his experience on the experimental measurements as well as for the stimulating discussions, L. Bottura and P. Fessia for believing in this project, B. Colijn, J. van Nugteren and L. Hincapie Galeano for the help in the computer simulations, B. Baudouy, R. van Weelderen and C. Meuris for the fruitful discussions and suggestions. The author is also grateful to S. Luzieux, A. Bonasia, P. Jacquot, S. Clement, A. Benfkih and J.-L. Carpano for collaborating in the samples preparation.

References

[1] Burnod L, Leroy D, Szeless B, Baudouy B, Meuris C. Thermal modeling of the LHC dipoles functioning in superfluid helium. In: Proceedings 4th European particle accelerator conference EPAC '94, London, England; 1994. p. 2295–7.
[2] van Weelderen R, Vullierme B, Peterson T. The cryogenic design of the phase I upgrade inner triplet magnets for LHC. In: Proceedings of ICEC 23 – ICMC 2010, Wroclaw, Poland; 2010. p. 899–903.
[3] Meuris C, Baudouy B, Leroy D, Szeless B. Heat transfer in electrical insulation of LHC cables cooled with superfluid helium. Cryogenics 1999;39:921–31.
[4] Jaffrey TS et al. Fermilab-built SSC collider dipoles using low temperature curing insulation systems with and without glass tape. In: Proceedings 15th particle accelerator conference PAC '93, Washnigton DC, USA; 1993. p. 2769–71.
[5] Bottura L, de Rijk G, Rossi L, Todesco E. Advanced accelerator magnets for upgrading the LHC. IEEE Trans Appl Sup 2012;22(3):4002008.
[6] La China M, Tommasini D. A comparative study of heat transfer from Nb–Ti and Nb_3 Sn coils to He II. Phys Rev Spec Top Accel Beams 2008;11:082401.
[7] Kirby G et al. Engineering design and manufacturing challenges for a wide-aperture, superconducting quadrupole magnet. IEEE Trans Appl Sup 2012;22(3):4001804.
[8] Meuris C. Heat transport in insulation of cables cooled by superfluid helium. Cryogenics 1991;31:624–8.
[9] Kimura N, Kovachev V, Nakamoto T, Yamamoto A, Shintomi T, Terashima A, et al. Heat transfer from insulated Rutherford type cables immersed in pressurized He II. Adv Cryogenic Eng 1998;43:1433–40.
[10] Kimura N, Yamamoto A, Shintomi T, Terashima A, Kovachev V, Murakami M. Heat transfer characteristics of Rutherford-type superconducting cables in pressurized He II. IEEE Trans Appl Sup 1999;9(2):1097–100.
[11] Richter D, Fleiter J, Baudouy B, Devred A. Evaluation of the transfer of heat from the coil of the LHC dipole magnet to helium II. IEEE Trans Appl Sup 2007;17(2):1263–8.
[12] Granieri PP, Fessia P, Richter D, Tommasini D. Heat transfer in an enhanced cable insulation scheme for the superconducting magnets of the LHC luminosity upgrade. IEEE Trans Appl Sup 2010;20(3):168–71.
[13] Granieri PP. Heat transfer between the superconducting cables of the LHC accelerator magnets and the superfluid helium bath. Ph.D. dissertation, Swiss Federal Institute of Lausanne (EPFL) and CERN; 2012.
[14] Baudouy B, François MX, Juster F-P, Meuris C. He II heat transfer through superconducting cables electrical insulation. Cryogenics 2000;40:127–36.
[15] Bruning O et al. LHC Design Report, vol. 1, CERN, Geneva, Switzerland; 2004. p. 157.

[16] Baudouy B. Kapitza resistance and thermal conductivity of Kapton in superfluid helium. Cryogenics 2003;43:667–72.
[17] Lawrence J, Patel AB, Brisson JG. The thermal conductivity of Kapton HN between 0.5 and 5 K. Cryogenics 2000;40:203–7.
[18] National Institute of Standards and Technology (NIST), website: <http://www.nist.gov/index.html>.
[19] CRYOCOMP version 3, Eckels Engineering Inc.
[20] Barucci M, Gottardi E, Peroni I, Ventura G. Low temperature thermal conductivity of Kapton and Upilex. Cryogenics 2000;40:145–7.
[21] Benford DJ, Powers TJ, Moseley SH. Thermal conductivity of Kapton tape. Cryogenics 1999;39:93–5.
[22] Kimura N, Nakai H, Murakami M, Yamamoto A, Shintomi T. A study of the heat transfer properties of pressurized helium II through fine channels. Adv Cryogenic Eng 2006;51:97–104.
[23] Granieri PP, Baudouy B, Four A, Lentijo F, Mapelli A, Petagna P, et al. Steady-state heat transfer through micro-channels in pressurized He II. Adv Cryogenic Eng 2012;1434:231-238.
[24] Bejan A. Convection heat transfer. 2nd ed. New York: John Wiley & Sons, Inc.; 1995. p. 105.
[25] Van Sciver SW. Helium cryogenics. New York and London: Plenum Press; 1986. p. 116.
[26] HEPAK, Cryodata, Inc., P.O. Box 173, Louisville, CO 80027.
[27] Ladner DR, Tough JT. Temperature and velocity dependence of superfluid turbulence. Phys Rev B 1979;20(7):2690–701.
[28] Gmelin E, Asen-Palmer M, Reuther M, Villar R. Thermal boundary resistance of mechanical contacts between solids at sub-ambient temperatures. J Phys D: Appl Phys 1999;32:19–43.
[29] Fessia P, Granieri PP, et al. Electrical and mechanical performance of an enhanced cable insulation scheme for superconducting magnets. IEEE Trans Appl Sup 2010;20(3):1622–5.
[30] Granieri PP, Fessia P, Richter D, Tommasini D. Thermally enhanced cable insulation for the Nb–Ti high luminosity LHC inner triplet mode. IEEE Trans Appl Sup 2012;22(3):7700404.
[31] Fessia P, Kummer H, Kuribayashi H, Tommasini D, Van de Velde F. Curing of LHC main dipole coils insulated with all polyimide PIXEO® adhesive tape. IEEE Trans Appl Sup 2006;16(2):1782–5.
[32] Baudouy B. Etude des transferts de chaleur dans les isolations électriques de câbles supraconducteurs d'aimant d'accélérateur refroidi par hélium superfluide. Ph.D. dissertation, Université Pierre et Marie Curie and CEA-Saclay; 1996.
[33] Chorowski M, Polinski J, Strychalski M. Heat transfer through Rutherford superconducting cable with novel pattern of polyimide electrical insulation in pressurized superuid helium environment. Adv Cryogenic Eng 2012;1434:255-262.
[34] Bocian D, unpublished calculation.
[35] Bielert E, Verweij A, ten Kate H. Finite element modeling in 3D of the impact of super uid helium filled micro-channels on the heat transfer through LHC type cable insulation. IEEE Trans Appl Sup 2012;22(3):4701205.
[36] Lorin C, unpublished calculation.